

Contents lists available at ScienceDirect

# Journal of Wind Engineering & Industrial Aerodynamics

journal homepage: www.elsevier.com/locate/jweia



# Damage assessment of wood frame shear walls subjected to lateral wind load and windborne debris impact



Dikshant Saini, Behrouz Shafei

Department of Civil, Construction, and Environmental Engineering, Iowa State University, Ames, IA, 50011, USA

#### ARTICLE INFO

Keywords:
Wood frame shear wall
Lateral wind load
Windborne debris
Damage analysis
Residual capacity
Multi-hazard assessment

#### ABSTRACT

A number of studies have been performed to understand the lateral load carrying capacity of wood frame shear walls. The existing studies, however, have been primarily focused on the intact shear walls, disregarding the possibility of capacity loss due to prior extreme loading events. During windstorms, in particular, windborne debris is the leading cause of damage and destruction. While the impact force induced by windborne debris can directly damage a shear wall, the consequences can become disastrous, as the prior damage adversely affects the in-plane lateral load carrying capacity of the shear wall. This critical aspect motivated the current study to investigate the impact and post-impact performance of wood frame shear walls. For this purpose, a high-fidelity computational framework capable of characterizing both types of damage is developed. Further to providing an in-depth understanding of the process of damage formation and propagatin, this study examines how a range of impact scenarios and wall design factors influence the extent of damage that the wood frame shear walls experience in a windstorm. The outcome of this study is then employed to introduce a capacity loss index for the multihazard design and assessment of wood frame (and other similar) shear walls in the regions prone to severe windstorms.

# 1. Introduction

During tornados and hurricanes, windborne debris is known to be one of the main causes of damage to lightweight residential and commercial building structures, incurring billions of dollars of property loss every year. Common windborne debris objects are roof gravels, shingles, tiles, tree limbs, rafters, and framing members, which can be broadly categorized to "unrestrained" and "failed" objects (Lin et al., 2007). Large missiles, such as tree limbs and framing members, often travel at (relatively) low velocities. However, they can induce extensive damage to exterior walls due to their (relatively) high mass. For the design of building envelope components, including exterior walls, against windborne debris hazard, a number of guidelines/standards have been developed (e.g., FBC, 2017; FEMA, 2015; ICC, 2014). Among them, FEMA (2015) and ICC (2014) provide similar details for the assessment of the risk of windborne debris impact. The debris impact velocity is assumed to vary based on the design wind speed, shelter type, and impact location. For the impact resistance assessment of wall panels, FBC (2017) prescribes a test missile of 4.1 kg (9 lb.) with the nominal cross-sectional dimensions of 50 mm  $\times$  100 mm (2 in.  $\times$  4 in.). The debris mass can increase to 6.8 kg (15 lb.) for tornado-borne debris, while the debris dimensions remain the same (ICC, 2014). The procedure and apparatus required for the impact tests are provided in ASTM E1886 (2013) and ASTM E1996 (2017). While these guidelines/standards are widely used in the industry to test building envelope products against windborne debris impact, their scope is rather limited, as many of wind load characteristics and debris trajectory details are disregarded. This issue has been explored through the past studies devoted to improving the debris flight models under strong winds.

The current body of knowledge on debris flight (prior to impact) can be broadly divided to experimental (e.g., Tachikawa, 1988; Holmes, 2004; Holmes et al., 2006; Lin et al., 2006, 2007; Visscher and Kopp, 2007; Kordi et al., 2010; Kordi and Kopp, 2011), analytical (e.g., Tachikawa, 1983; Wills et al., 2002; Holmes, 2004; Lin et al., 2007; Baker, 2007; Richards et al., 2008; Noda and Nagao, 2010; Baker and Sterling, 2017), and computational (e.g., Andersen et al., 2005; Jin and Xu, 2008; Kakimpa, 2012 a,b) investigations. The cited studies all agree that debris trajectories are sensitive to a variety of factors, such as local topography and turbulence, as well as support and launch conditions. Focusing on the impact resistance of wall panels, a number of studies have explored structural panels (e.g., Alphonso and Barbato, 2014; Herbin and Barbato, 2012; Pathirana et al., 2017; Saini and Shafei, 2018)

E-mail addresses: dikshant@iastate.edu (D. Saini), shafei@iastate.edu (B. Shafei).

<sup>\*</sup> Corresponding author.

and composite structural insulated panels with different front and back skin types (e.g., Chen and Hao, 2014, 2015; Hao et al., 2015). However, very few investigations have been carried out on the impact resistance of wood frame shear walls, which are commonly used in lightweight structural systems, especially in North America.

The penetration of debris into a wall causes local damage, leading to changes in the internal pressure of the building. The situation, however, becomes critical if the impacted wall is expected to serve as a shear wall. The local damage results in the loss of in-plane lateral load carrying capacity of the shear wall, which makes the entire building structure vulnerable to collapse under wind-induced loads. Such a domino effect has been confirmed in the past reconnaissance studies performed on wood frame shear walls after windstorms (Oliver and Hanson, 1992; Marshall, 2002; FEMA P-2022, 2019). This demands a multi-hazard design and assessment platform for wood frame shear walls subjected to windborne debris and lateral wind loads. There is, however, no systematic study in the literature regarding the combination of loads that the wood frame shear walls experience, particularly if used in the regions prone to strong winds. This was one of the main motivations of the current study to not only assess the wood frame shear walls under windborne debris hazard, but also investigate their in-plane performance after an impact-induced damage occurs.

Wood frame structures often consist of horizontal diaphragms in conjunction with shear walls to resist both gravity and lateral loads (van de Lindt, 2004). The shear walls are made of dimensional or engineered lumbers surfaced with structural sheathing panels, such as oriented strand board (OSB), plywood, and gypsum board. The performance of intact wood frame shear walls under lateral loads has been investigated through a number of experimental and numerical studies (e.g., Gupta and Kuo, 1985; Lam et al., 1997; Folz and Filiatrault, 2001; Gatto and Uang, 2003; Blasetti et al., 2008; Pei et al., 2012; Lafontaine et al., 2017; Wang et al., 2017). Based on the existing literature, the frame to sheathing panel connections govern the wall's overall structural response against lateral loads, while the studs and sheathing panels play an important role in defining the load-deformation properties. In a full-scale study conducted by Pei et al. (2012), the in-plane collapse limit of wood frame shear walls was evaluated. The results revealed that the tested walls can remain stable up to an interstory drift ratio in the range of 7%-10%. Lafontaine et al. (2017) performed full-scale laboratory tests to understand the lateral behavior of wood frame shear walls with gypsum sheathing panels. The response was found to become brittle when the nail spacing at the panel edges was reduced from 150 mm to 50 mm. In a separate effort, Wang et al. (2017) investigated the lateral load carrying capacity of lightweight shear walls made with laminated bamboo stud frames and ply-bamboo sheathing panels. The experimental test results revealed how the expected capacity can be influenced by the connection details and sheathing panel properties. In the absence of multi-hazard experiments in the current literature, the observations from separate impact and lateral load tests highlight the importance of employing an alternative computational framework that can capture all the necessary structural details, further to simulating various load effects, in such a way that a holistic vulnerability assessment can be achieved.

To evaluate the performance of wood frame shear walls under realistic exposure conditions, involving both windborne debris impact and lateral wind load, a high-fidelity computational framework is developed in the current study. This framework is capable of characterizing two critical aspects: (1) the extent of damage due to debris impact, taking into account the high strain rate nature of the phenomenon, and (2) the consequences of impact-induced damage, quantifying the residual load carrying capacity of wood frame shear walls. For this purpose, rigorous finite-element (FE) models are developed and validated with the single-hazard experimental test results. The impact simulations are then performed on a set of representative wood frame shear walls to determine the key impact response characteristics, such as debris penetration depth, extent of damage, and energy absorption capacity. The impact scenarios are designed to cover various contributing factors, such as angle of

impact, impact velocity, nail spacing, and wall's moisture content. Upon obtaining an in-depth understanding of the vulnerability of wood frame shear walls to windborne debris hazard, in-plane lateral wind loads are applied to the shear walls. For this purpose, the simulations are performed on the FE models that carry the damage induced by debris impact. The outcome of the second set of simulations leads to a capacity loss index that quantifies what percentage of the original lateral load carrying capacity of wood frame shear walls is lost due to windborne debris impact. This is expected to pave the way for multi-hazard design and assessment of wood frame (and other similar) shear wall systems in the regions prone to severe windstorms.

### 2. Numerical models for wood frame shear walls

Detailed FE models are developed for a set of representative wood frame shear walls to evaluate their structural response to windborne debris impact and subsequent wind-induced lateral loads. A description of the geometry of the wood frame shear walls under consideration, material models, and loading scenarios is provided in this section.

# 2.1. Details of wood frame shear walls

In this study, the performance of wood frame shear walls with OSB sheathing panels is investigated. Such walls are commonly used in prefabricated residential and commercial building structures. The shear walls under consideration often come in the form of 2.4 m  $\times$  2.4 m panels (Durham et al., 2001). The framing members are assumed to be made of pine lumbers with a cross-sectional dimension of 38 mm  $\times$  89 mm. The framing members are connected by 75 mm long nails. The studs are spaced at 400 mm center to center and have been connected to horizontal framing members at both top and bottom. All the individual studs are allowed to rotate at their ends (in both in-plane and out-of-plane directions) with a partial restraint due to the presence of nails. This ensures capturing the response of the walls in a realistic way, including possible separations of the individual studs from the bottom framing member due to the weak withdrawal capacity in the nails. It is critical to note that only the base of the bottom framing member has been rigidly fixed (because of the anchorages). The sheathing panels, which have a 9.5 mm thickness, are connected to the framing members with pneumatically-driven spiral nails. The nails under consideration are 50 mm long with a diameter of 2.67 mm. Noting the significant effect of frame to sheathing panel connection details on lateral load carrying capacity, three different configurations of wood frame shear walls (i.e., N1, N2, and N3 Walls) are considered in the current study based on the nail spacing along the interior studs and the left and right edges of the sheathing panel, where the end studs are located. For the N1 Wall, a nail spacing of 300 mm and 150 mm is used along the interior and end studs, respectively. For the N2 Wall, the nail spacing of the interior stude is reduced to half, i.e., 150 mm, while maintaining the nail spacing of the end studs. It should be noted that the effect of nail spacing at interior studs is less pronounced compared to panel edges. However, this is still an important parameter, as reported in the study completed by Tissell (1993). Finally, for the N3 Wall, while maintaining the nail spacing of the interior studs similar to the N1 Wall, the nail spacing of the end studs is reduced to half, i.e., 75 mm. As summarized in Table 1, this provides realistic combinations of nail spacing at the interior and end studs. Fig. 1 shows a sketch of the wood frame shear walls under consideration and the FE models developed for them in this study. For debris impact simulations, a typical timber projectile with a mass of 4.1 kg and cross-sectional dimensions of 50 mm  $\times$  100 mm (2 in.  $\times$  4 in.) is used. This satisfies the requirements for extreme test conditions per Florida Building Code (FBC, 2017). It is important to mention that while 50 mm  $\times$  100 mm (2 in.  $\times$  4 in.) are the rough cut dimensions of the timber projectile, as reported in the past experimental tests (Chen and Hao, 2014, 2015; Meng et al., 2016 a,b), the actual dimensions are smaller than 50 mm  $\times$  100 mm (2 in.  $\times$  4 in.).

The wood frame shear wall models consist of all the essential com-

 Table 1

 Wood frame shear wall configurations investigated in the current study.

	Nail Spacing (mm)		Moisture Content	
Wall	Interior Studs	End Studs		
			5%	
N/1	200	150	10%	
N1	300	150	15%	
			20%	
N2	150	150	10%	
N3	300	75	10%	

ponents, including framing members, sheathing panel, and mechanical fasteners. Eight-node solid elements (with three degrees of freedom per node) are used to model the framing members and sheathing panels. Such elements are particularly appropriate to model the structural elements that are susceptible to experience a negative volume. Considering that wood is a complex material with orientation-dependent stiffness and strength, a detailed model is essential to accurately capture the stressstrain relationships and failure modes, as they are influenced by the type and direction of the applied load relative to the grains. In this study, an elastic plastic wood model is employed to take into account the properties of wood parallel and perpendicular to grains. The model includes both hardening and softening formulations to simulate the stressstrain relationship. While this relationship provides ductility in compression, it remains linear until brittle failure in tension and shear. The nonlinear response of the wood under tension and compression is primarily controlled by the fracture energies parallel and perpendicular to grains. Under compression, the post peak transition behavior is governed by the initial yield surface location and rate of translation. The material model also considers the effect of strain rate in the constitutive equations and damage formulations. Further details regarding the wood material model can be found in Murray (2007). For predicting the failure, two yield functions, i.e.,  $f_{\parallel}$  and  $f_{\perp}$ , are defined in parallel and perpendicular to the grain direction, respectively:

$$f_{\parallel} = \frac{\sigma_{11}^2}{X^2} + \frac{\sigma_{12}^2 + \sigma_{13}^2}{S_{\parallel}^2} - 1 \quad \text{and} \quad X = \begin{cases} X_T & \text{for } \sigma_{11} \ge 0 \\ X_C & \text{for } \sigma_{11} < 0 \end{cases}$$
 (1)

$$f_{\perp} = \frac{\sigma_{22}^2 + \sigma_{33}^2}{Y^2} + \begin{array}{cc} \frac{\sigma_{23}^2 - \sigma_{22}\sigma_{33}}{S_{\perp}^2} - 1 & \text{and} & Y = \begin{cases} Y_T & \text{for} & \sigma_{22} + \sigma_{33} \ge 0 \\ Y_C & \text{for} & \sigma_{22} + \sigma_{33} < 0 \end{cases}$$

where  $X_T$  and  $Y_T$  are the tensile strength parallel and perpendicular to the wood grains, respectively;  $X_C$  and  $Y_C$  are the compressive strength parallel and perpendicular to the wood grains, respectively; and  $S_{\perp}$  and  $S_{\perp}$ are the shear strength parallel and perpendicular to the grain direction, respectively (LSTC, 2016). In Equations (1) and (2),  $\sigma_{11}$ ,  $\sigma_{22}$ , and  $\sigma_{33}$  are the stresses along the three orthogonal directions. Since wood is a hygroscopic material, it is capable of absorbing moisture during its service life. The wood's moisture content can significantly influence the performance of wood frame shear walls. Thus, four moisture contents, ranging from 5% to 20% (in 5% intervals), are considered for the framing members in the current study to quantify the effect of this critical factor. The stated range is consistent with the range suggested by Glass and TenWolde (2007), which performed a holistic review of the past studies on the in-service moisture and temperature condition of wood frame buildings. The input parameters required for the wood material model are provided in Table 2, which has been adopted from the investigations performed by Otkur (2010).

The OSB sheathing panel is connected to the framing members using a set of nails. Discrete spring elements with nonlinear properties are used to model the behavior of nail connections with necessary details. The force-displacement  $(P-\Delta)$  relationship for the frame to sheathing panel connections is modeled using a logarithmic expression with a linear softening branch:

$$P = \begin{cases} P_{o} + r_{1}K_{o}\Delta\left(1 - e^{\frac{-K_{o}\Delta}{P_{o}}}\right) & \text{if } \Delta \leq \Delta_{\text{ult}} \\ P_{\text{ult}} + r_{2}K_{o}(\Delta - \Delta_{\text{ult}}) & \text{if } \Delta_{\text{ult}} < \Delta \leq \Delta_{\text{fail}} \end{cases}$$
(3)

where  $K_0$  is the initial stiffness (0.561 kN/m);  $P_0$  is the secondary stiffness intercept on the Y axis (0.751 kN);  $P_{\rm ult}$  is the ultimate load corresponding to the ultimate displacement,  $\Delta_{\rm ult}$  (12.5 mm);  $\Delta_{\rm fail}$  is the failure displacement; and  $r_1$  and  $r_2$  are the fitting coefficients (0.061 and -0.078, respectively), all obtained from the experimental test data reported by Durham et al. (1998). As noted in the past impact experiments and field observations, the hardwood projectile commonly experiences no deformation or mass loss during impact. Thus, it is modeled as a rigid object in the current study. It should be mentioned that using a rigid material for the hardwood projectile neglects the elastic energy transferred to the projectile after impact and may produce a small overestimation of the energy dissipated by the wood frame shear wall, particularly for low impact velocities when rebounding of the projectile

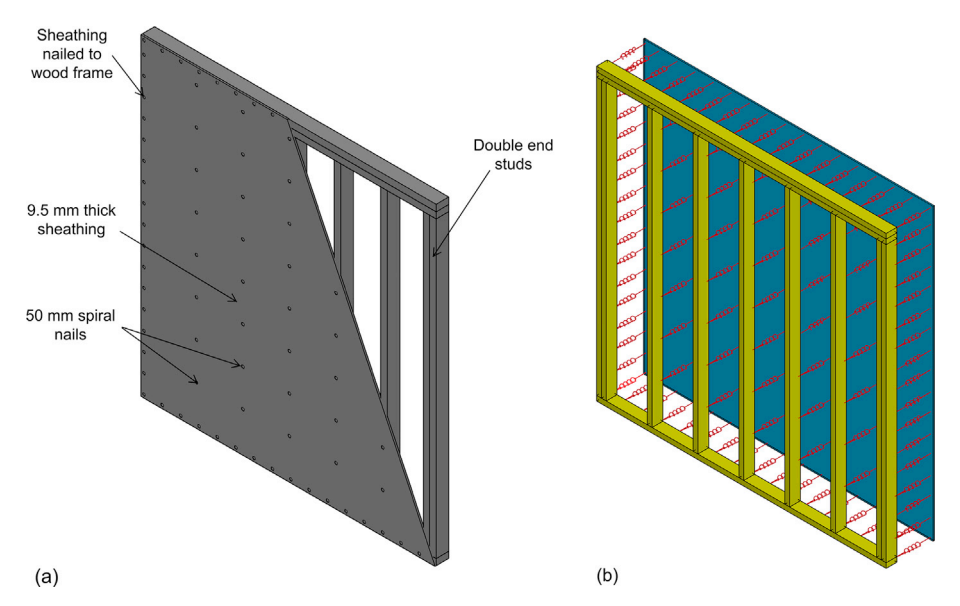


Fig. 1. Wood frame shear walls under consideration: (a) schematic sketch, and (b) developed FE model.

**Table 2**Material properties of the southern pine lumbers (as a function of moisture content) and OSB sheathing panels.

Property	Southern Pine Lumbers				Sheathing Panels
Moisture Content	5%	10%	15%	20%	OSB
Density (kg/m³)	673.1	673.1	673.1	673.1	638.0
Parallel normal modulus (MPa)	16340	15490	14231	12560	3500
Perpendicular normal modulus (MPa)	979.0	910.1	737.7	461.9	1800.0
Parallel shear modulus (MPa)	805.0	789.8	767.0	836.9	1100.0
Perpendicular shear modulus (MPa)	357.7	332.3	267.6	165.5	1100.0
Parallel major Poisson's ratio	0.2860	0.2586	0.2246	0.1842	0.2000
Parallel tensile strength (MPa)	57.29	66.19	64.55	52.38	9.90
Parallel compressive strength (MPa)	46.72	37.00	27.61	18.58	15.90
Parallel shear strength (MPa)	9.19	8.53	7.32	5.58	6.80
Perpendicular tensile strength (MPa)	1.92	2.14	1.98	1.46	7.20
Perpendicular compressive strength (MPa)	8.89	7.14	5.38	3.63	12.90
Perpendicular shear strength (MPa)	12.87	11.94	7.32	7.81	6.80

is likely (Herbin and Barbato, 2012). The comparison of simulation results performed with both rigid and elastic projectile confirms that the difference in all the key response measures remains marginal. To control the interactions between the projectile and the wood frame shear wall, an eroding surface to surface contact algorithm with a segment-based capability is employed (Saini and Shafei, 2019 a-c). In addition, an eroding single surface contact algorithm is used to control the interactions between the studs and the sheathing panel. Considering the high strain rate nature of the event, an interior contact is also included to avoid the formation of a negative volume in the studs or the sheathing panel.

# 2.2. Validation of numerical models under both lateral wind and impact loads

To ensure that the developed FE models provide accurate results under debris impact, the validation study begins from the cannon test results performed on similar wood panels. Chen and Hao (2015) carried out a series of laboratory experiments using a pneumatic cannon system to investigate the impact resistance of OSB skin structural insulated panels. In the experiments, the panels were impacted by 4.0 kg hardwood projectiles with cross-sectional dimensions of 50 mm  $\times$  100 mm. In the current study, a numerical model that replicates the panels is developed in the LS-DYNA software package and various structural response measures, such as displacement, penetration depth, and failure mode, are examined. Considering the fact that the panel is symmetric in both horizontal and vertical directions, a quarter of the panel is modeled to reduce the computational effort. Eight-node solid elements with single-point integration are employed to model the panel. A detailed mesh convergence study is conducted in the beginning to confirm that the simulation results converge to a unique solution and are independent of mesh size. This leads to a (relatively) fine mesh for the impact region and a (relatively) coarse mesh for the regions away from it. Fig. 2 illustrates the projectile's velocity time-history when it impacts the end stud of the N1 Wall. Four different element sizes of 15.0 mm, 10.0 mm, 5.0 mm, and 2.5 mm are tested for the region of impact. The mesh size in the rest of the panel, i.e., outside the region of impact, is maintained equal to 20.0 mm for all the four cases. As demonstrated in Fig. 2, a significant difference in the projectile velocity is observed when the two large mesh sizes are employed. However, with decreasing the mesh size to 5.0 mm and 2.5 mm, it is noted that the results become insensitive to the mesh size. Thus, to achieve computational efficiency while maintaining the accuracy of results, a mesh size of 5.0 mm was adopted for the subsequent FE simulations

Fig. 3(a) shows the failure pattern extracted from the numerical simulation. The simulated panel experiences a shear failure upon the creation of a rectangular hole, which is consistent with the observations made during the experiment. In addition, Fig. 3(b) illustrates how the displacement time history recorded at half distance between the center and top edge of the panel varies between the experiment and simulation. A peak displacement of 8.7 mm is obtained from the FE simulation in comparison with 9.0 mm reported from the experiment. Further to capturing the peak displacement, the simulation is found to properly reflect the overall trend of the displacement time history measured during the experiment. This confirms that the developed FE models produce accurate predictions for the wall panels subjected to debris impact. The small discrepancy observed in the residual displacement originates from the edge support conditions. In the experimental test setup, each specimen was attached to a steel frame using G-clamps. This boundary condition was converted in the FE models to constraints against translation in the three orthogonal directions at the four edges.

The developed FE models are then validated with the full-scale test results that involve in-plane lateral loads applied to intact wood panels (in the absence of similar experiments on damaged panels). The lateral load carrying capacity is evaluated by applying a horizontal displacement to the top framing member of the wall panel. Hold-downs and anchorages are often used in practice for connecting the wall to the foundation or floor below. They are primarily intended to prevent the uplift and sliding of the wall at its base, thus, the base of the bottom framing member is assumed to be constrained against all degrees of freedom. Upon replicating the structural details, load-displacement curves are generated for the same setup tested by Durham et al. (1998). An investigation of the damaged wall panel shows that failure begins from bottom corners, as reflected in Fig. 4(a). This is consistent with the observations made during the experiment. Fig. 4(b) indicates that the developed FE model can predict both ultimate load and load-displacement relationship in a good agreement with the experiment. The ultimate load is found to be 25.21 kN in comparison to 21.94 kN from the experiment (with 14.9% difference), while the displacement at the ultimate load is observed to be 47.9 mm in comparison to 54.63 mm from the experiment (with 12.3% difference). Despite properly capturing the main structural response characteristics, the accuracy of predictions could be further improved

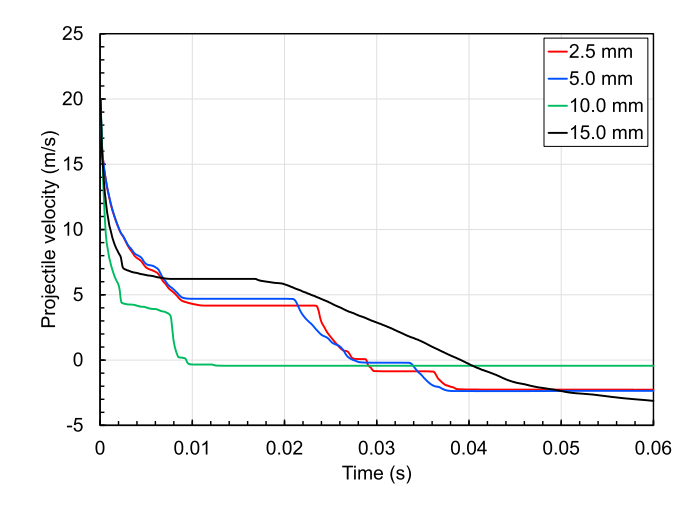
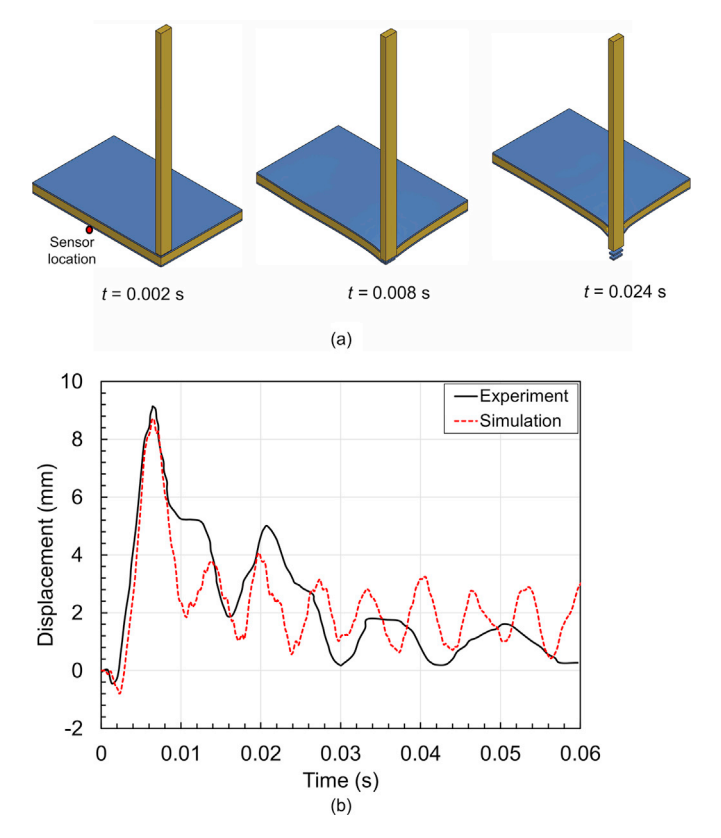


Fig. 2. Debris velocity time histories obtained with different mesh sizes for an impact at the end stud of the N1 Wall.



**Fig. 3.** Results from debris impact analysis: (a) time-dependent deformed shapes, and (b) comparision of the load-displacement curves obtained from the experiment and FE simulation.

with the availability of more detailed information for OSB material properties and their connections to the framing members.

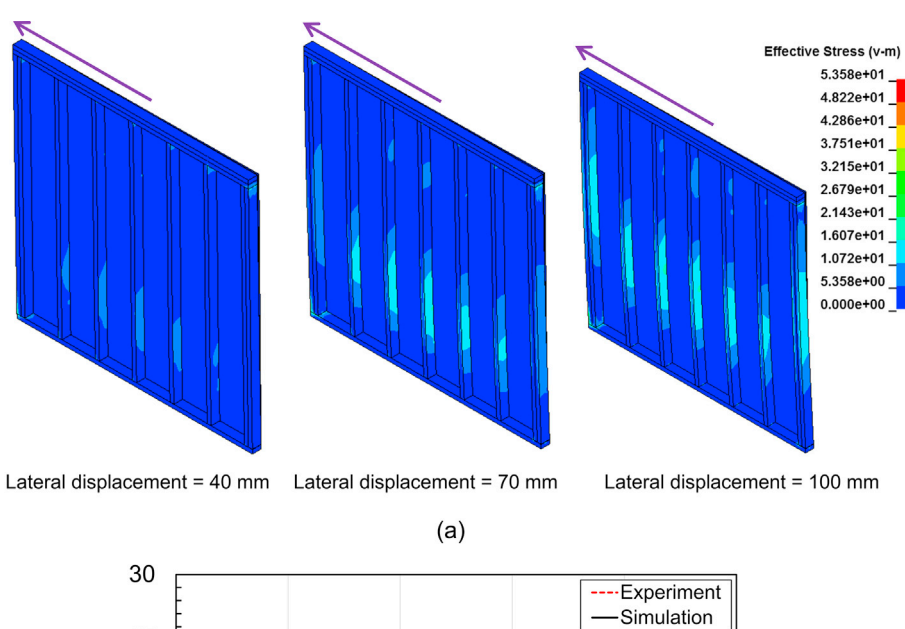
# 3. Vulnerability to debris impact

The wood frame shear walls under consideration are subjected to a number of debris impact scenarios to evaluate the extent of impactinduced deformation and damage. To define the debris impact scenarios, the current codes/guidelines relevant to windborne debris impact, such as ICC (2014), FEMA (2015), and FBC (2017), are considered. According to FBC (2017), the wall panels need to be tested under an impact velocity of 24.4 m/s for the structures in Risk Category IV. For the structures in the other risk categories, the impact velocity can be reduced to 15.2 m/s. To obtain a holistic vulnerability assessment, the current study covers a wide range of impact locations (i.e., end stud, central stud, and sheathing panel), impact velocities (i.e., from 5.0 m/s to 30.0 m/s in 2.5 m/s intervals), and angles of attack (i.e., from 45° to 90° in 15° intervals). For each impact location, the penetration depth of the projectile is measured as one of the parameters used for damage assessment. Fig. 5 compares the penetration depth of the debris into the N1 Wall impacted at different locations with different impact velocities (under a 90° angle of attack). The penetration depth is found to consistently increase with increasing the impact velocity until failure. Under the impact velocities ranging from 5.0 m/s to 15.0 m/s, the central stud undergoes less displacement than the end stud because the end stud is supported only on one side, while the central stud is supported on both sides, reducing the extent of debris penetration. The end stud, however, is able to resist higher impact velocities, as it is made of two framing members with a smaller nail spacing (i.e., 150 mm instead of 300 mm in the N1 Wall). The end stud is found to fail at an impact velocity of 25.0 m/s, while the central stud fails at 17.5 m/s marked by the detachment of the stud from the wall. For the central stud, it is noted that the penetration depth

significantly increases with changing the impact velocity from 15.0 to 17.5 m/s. From a detailed review of the progress of damage formation and propagation, this can be attributed to the failure of sheathing to central stud connections. An impact velocity of 15.5 m/s and 16.0 m/s results in the failure of two and four nails, respectively. When the impact velocity reaches 16.5 m/s, six nails fail, but the projectile penetration is still resisted, mainly because the central stud maintains its connection to the top and bottom horizontal framing members. With increasing the velocity beyond 17.0 m/s, however, the end connections are also lost and a full penetration occurs. Fig. 6 compares the deformed shape of the N1 Wall impacted at the end and central stud under an impact velocity of 20.0 m/s. This figure confirms that the central stud is completely detached from the wall, while the end stud remains in contact with the wall (despite the failure of a few nails). In addition to the impact on the central and end studs, simulations are carried out to capture the risk of debris impact on the sheathing panel. The sheathing panel is found to fail under a direct impact as soon as the debris impact velocity exceeds 10.0 m/s.

The debris impact simulations are further extended to the N2 and N3 Walls to understand the effect of nail spacing. Compared to the N1 Wall, the N2 and N3 Walls have a decreased nail spacing at their interior and end studs, respectively. To understand the effect of nail spacing in the interior studs, Fig. 7(a) shows the penetration depth under a debris impact at the central stud of the N1 and N2 Walls. For low impact velocities, i.e., between 5.0 m/s and 12.5 m/s, no significant difference is observed in the penetration depth of debris into the N1 and N2 Walls. However, the effect of nail spacing becomes pronounced as the impact velocity increases. For a velocity of 17.5 m/s, a penetration depth of 88.6 mm is observed in the N2 Wall, which is close to a third of the penetration depth recorded in the N1 Wall under the same impact velocity. To further understand the cause of this difference, Fig. 7(b) and (c) illustrate the number and fraction of failed nails as a function of debris impact velocity, respectively. With a failure of 86% of nails, the central stud of the N1 Wall is found to be detached from the wall at the 17.5 m/s impact velocity. The central stud of the N2 Wall, however, remains attached to the wall at the same impact velocity, as the fraction of failed nails is observed to be 60%, leaving enough nails in place to maintain the sheathing to central stud connection. For impact velocities higher than 17.5 m/s, the central stud is detached from both N1 and N2 Walls.

To understand the effect of nail spacing at the edge of the sheathing panel, Fig. 8(a) shows a comparison of penetration depth at the end studs of the N1 and N3 Walls. It is noted that the penetration depth can be reduced significantly if the nail spacing at the end studs is changed from 150 mm (for the N1 Wall) to 75 mm (for the N3 Wall). This is also reflected in the fact that the end stud in the N3 Wall can resist impact velocities up to 27.5 m/s (in contrast to maximum 22.5 m/s obtained for the N1 Wall). Fig. 8(b) and (c) compare the number and fraction of failed nails at the end stud of the N1 and N3 Walls at various impact velocities, respectively. Similar to Fig. 7, this figure indicates how a proper design of nail spacing can help ensure the proper transfer of the impact-induced forces in wood frame shear walls. The amount of energy absorbed during impact is employed as another measure to quantify the vulnerability of wood frame shear walls to windborne debris impact. Fig. 9(a) shows the time history of the main energy components in the simulation system when the end stud of the N1 Wall is subjected to a debris with an impact velocity of 20.0 m/s. While the kinetic energy of the impacted debris is found to decrease over time, the internal energy increases, reflecting the energy absorbed by the wall components. The energy absorption can originate from two phenomena in the wall, i.e., deformation and structural damage (Reddy et al., 1998). Fig. 9(b) illustrates how the total internal energy absorbed by the wall panel is distributed between the deformation and damage components. The energy absorption of the wood frame shear wall is observed to be mainly dominated by the wall's deformation. As the magnitude of the internal energy increases, however, the energy absorption due to structural damage increases. The hourglass energy, which captures the energy associated with the zero strain mode of the solid elements, is monitored throughout the simulations. With an



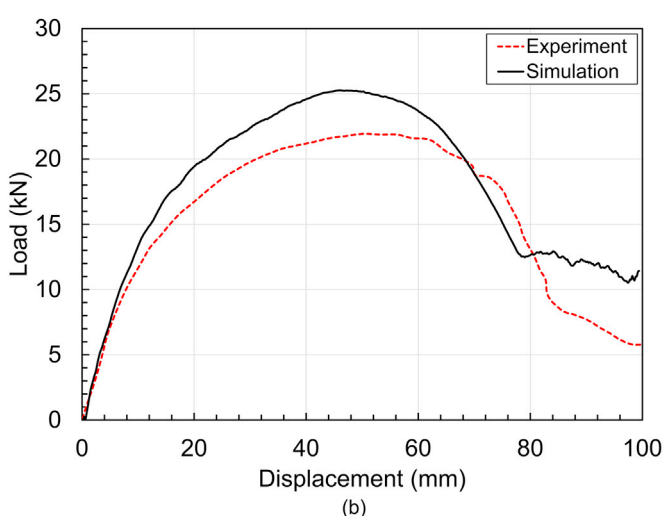
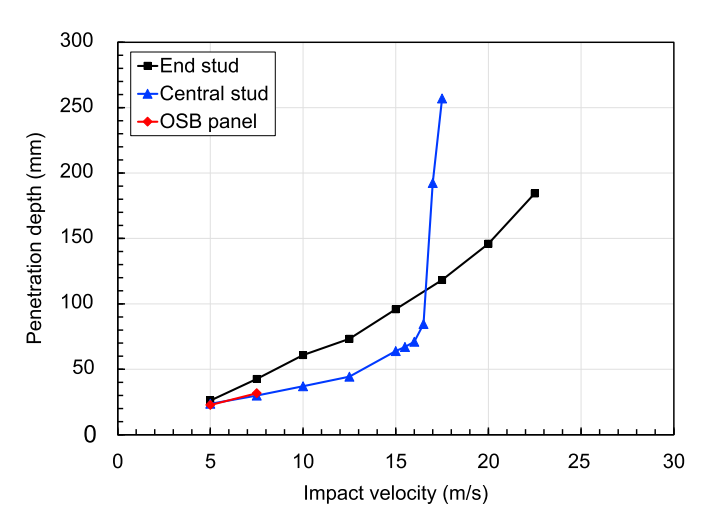


Fig. 4. Results from the in-plane pushover analysis: (a) deformed shapes under increasing displacements, and (b) comparision of the load-displacement curves obtained from the experimental test and FE simulation.



 ${\bf Fig.~5.}$  Penetration depth of the projectile into the N1 Wall impacted at three different locations.

hourglass energy not exceeding 10% of the total energy, it is ensured that the simulation results are not influenced by the hourglass effect.

# 4. Investigation of impact and wall design factors

To understand the effect of impact location, the energy absorption due to deformation and structural damage is further employed for the simulations performed on the N1 Wall subjected to windborne debris impact at the end and central studs. The energy absorption characteristics are found to vary depending on the point of impact. Fig. 10 illustrates the absorbed energy normalized with respect to the total energy for impact at the end and central studs. According to this figure, the energy absorbed due to deformation consistently decreases with increasing the impact velocity at the end stud. While the normalized energy absorbed due to deformation reduces from 0.89 to 0.42, the energy absorbed by structural damage is found to increase from 0.04 to 0.14. It should be noted that the total energy is not fully absorbed by the shear wall at high impact velocities. This fact, which is evident from the summation of the absorbed energy due to deformation and structural damage, means that the debris cannot be prevented from penetrating through the wall.

In the simulations performed to this point, the debris was considered

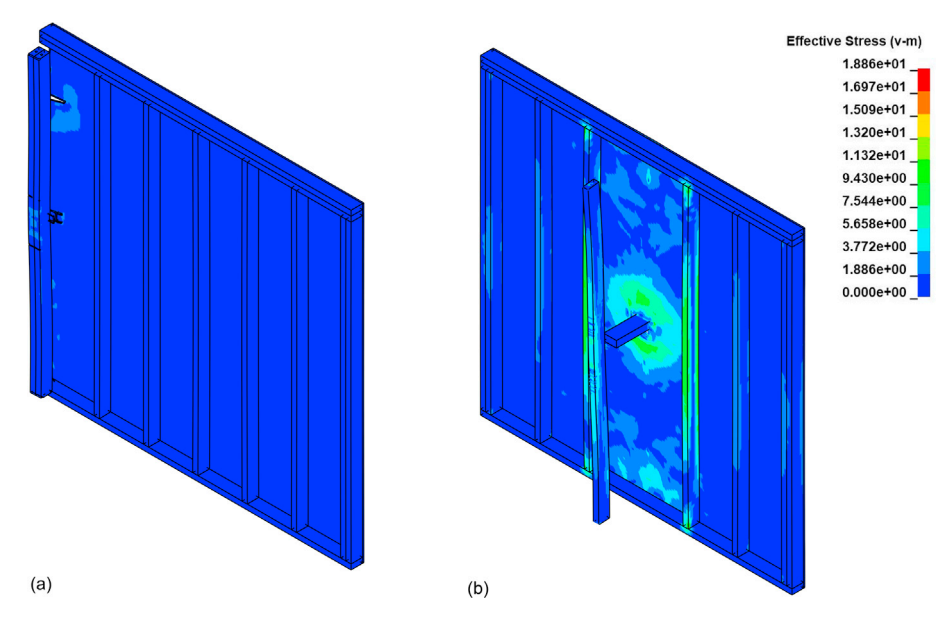


Fig. 6. Deformed shape of the N1 Wall under a 20.0 m/s debris impact at the (a) end stud, and (b) central stud.

to impact the wood frame shear wall with a 90° angle. However, the actual angle of debris impact can vary in hurricanes and tornadoes. To study this important factor, the simulations are extended to cover three additional angles of 75°, 60°, and 45°. Table 3 presents the debris penetration depth into the three walls impacted at the end stud with different angles of attack under a velocity of 20.0 m/s. For all the three walls, no significant difference is observed in the penetration depth between the 90° and 75° angles of attack. However, as the angle of attack is further reduced to 60° and 45°, the penetration depth decreases. This decrease is 13.4% and 27.9% in the N1 Wall for 60° and 45° angles of attack, respectively. Similar penetration depths are recorded for the N2 wall as the nail spacing of the N1 and N2 Walls is similar at the end stud, i.e., location of impact. On the other hand, the penetration depth into the N3 Wall impacted at the end stud is found least sensitive to the angle of attack. With decreasing the angle of attack to 60° and 45°, the penetration depth is found to experience a drop of only 8.5% and 13.2%, respectively. This can be associated to the close spacing of the nails in the end studs of the N3 Wall.

Further to the angle of impact, the moisture content of the wood panels is known to influence their performance under extreme loads. To quantify the effect of this factor, four moisture contents, i.e., 5%, 10%, 15%, and 20%, are considered for the central and end studs, in addition to the top and bottom framing members. Table 4 summarizes the debris penetration depths into the N1 Wall with different moisture contents. It is noted that the deformability of the studs increases with increasing the moisture content. This is characterized by their excessive deflections without undergoing a complete penetration. For an impact velocity of 20.0 m/s, the penetration depth increases from 145.9 mm to 164.5 mm, as the moisture content increases from 10% to 20%. The N1 Wall with 5% moisture content is found to fail at 20.0 m/s impact velocity, whereas the same wall with 20% moisture content does not undergo complete penetration even under an impact velocity of 25.0 m/s. The effect of moisture content is further investigated using the energy absorption characteristics of the N1 Wall, as shown in Fig. 11. It is clear that the absorbed energy due to deformation increases with increasing the moisture content. This can be attributed to increase in the wood's deformability with an increase in the moisture content. With changing the moisture content from 5% to 20%, the energy absorption due to the deformation of the impacted studs increases by 38% under an impact velocity of 20.0 m/s. On the other hand, the energy absorption due to damage remains almost the same under the same impact velocity.

Although an immediate determination of moisture content can be too difficult (with the current technology), the moisture content can be frequently checked during the service life of a building to obtain an assessment of the possible risk of failure during a windstorm. In a study conducted by Sherwood (1985), a test building was constructed near Gulfport, Mississippi, to monitor the moisture in the highly insulated walls used for the building envelope. It was found that the moisture content of the wall increased from 8-12% to 16–20% in two consecutive winters. If the buildings in service are equipped with the sensing systems that can monitor and report the moisture content, it is anticipated that not only more realistic assessments of the extent of vulnerability can be achieved, but also appropriate measures can be utilized to adjust the moisture content in such a way that the desired structural performance is achieved during windstorms.

# 5. Post-impact load carrying capacity

Because of the residual deformation and damage caused by windborne debris impact, the post-impact structural response of wood frame shear walls is adversely affected. To investigate this critical aspect, the inplane lateral load carrying capacity of the shear walls under consideration is evaluated by conducting a set of pushover analyses on the shear walls prior to and after debris impact. For this purpose, the shear walls are incrementally loaded in the transverse direction until the failure occurs. All the residual out-of-plane (and in-plane) deformations, as well as damage to the studs and sheathing panel, are systematically saved for each model at the end of each windborne debris impact simulation. The saved information is then loaded to the FE model prior to performing the simulations designed to assess the in-plane lateral load carrying capacity of the damaged shear walls. Fig. 12 (a)-(c) illustrates the loading pattern, as well as the deformed shape of the N1 Wall in two conditions: (i) intact, and (ii) damaged with a 20.0 m/s velocity debris impact. This figure shows how the deformation along the height of wall changes after an inplane lateral displacement of 70 mm is applied to the top of the wall. The lateral displacement has been further quantified in the displacement profile shown in Fig. 12(d). With the detachment of the central stud from the damaged wall, the lateral displacement is found to significantly increase throughout the wall panel. In addition to the deformed shapes, the load-displacement response of the walls is monitored during each simulation. Fig. 13 illustrates how the N1, N2, and N3 Walls respond to an increasing lateral displacement when they sustain a damage at the end

0.2

0 2.5 5 7.5

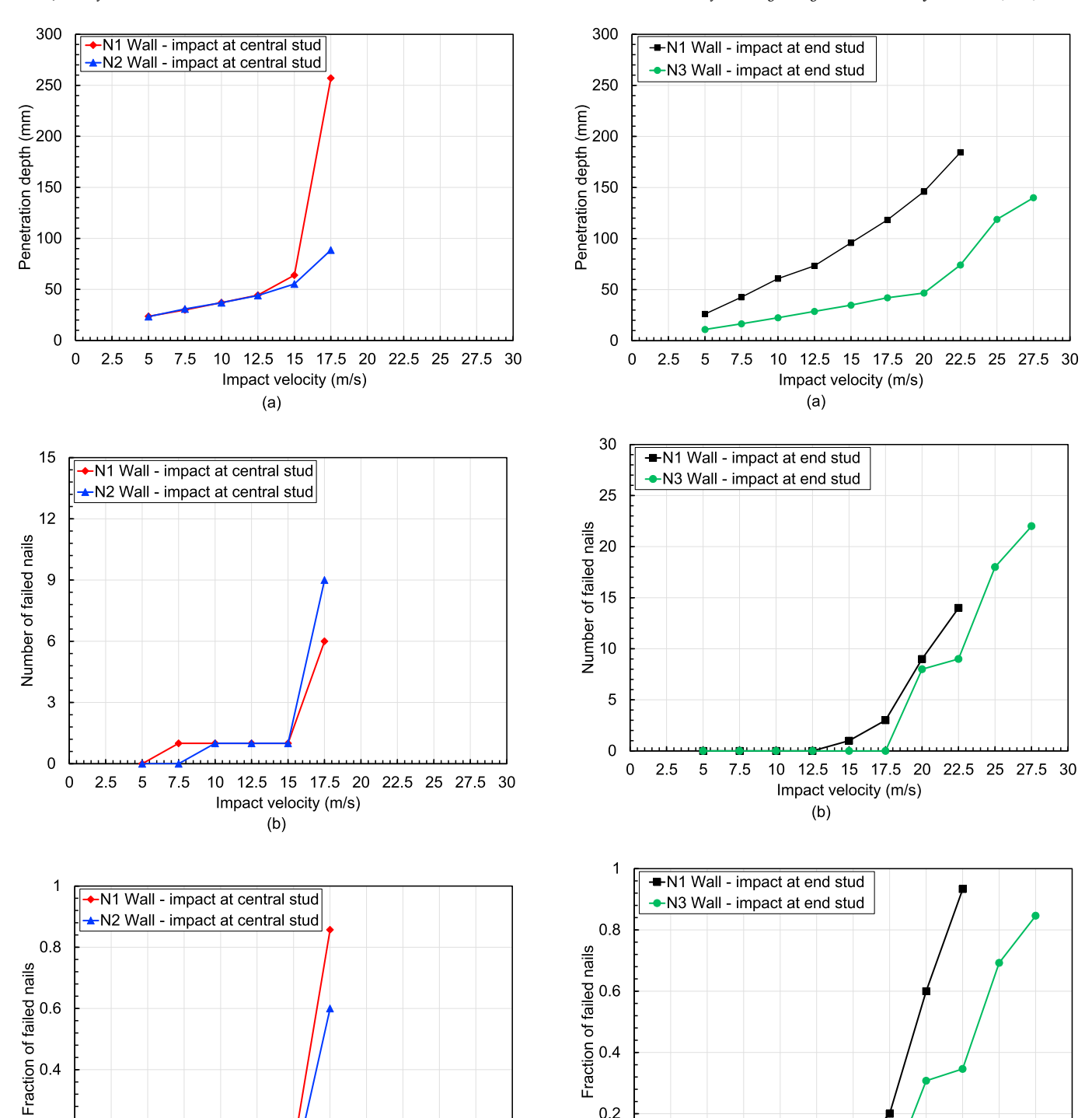


Fig. 7. Effect of nail spacing on the response of wall panels under debris impact at the central stud: (a) penetration depth, (b) number of failed nails, and (c) fraction of failed nails.

Impact velocity (m/s) (c)

10 12.5 15 17.5 20 22.5 25 27.5 30

stud (in comparison with the same walls in an intact condition).

The N1 Wall is found to provide an ultimate load carrying capacity of 25.2 kN at a lateral displacement of 47.2 mm. As a result of damage due

Fig. 8. Effect of nail spacing on the response of wall panels under debris impact at the end stud: (a) penetration depth, (b) number of failed nails, and (c) fraction of failed nails.

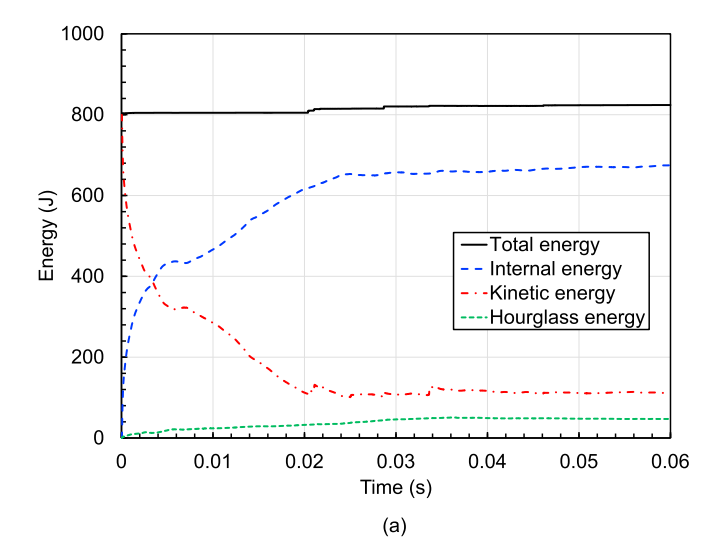
Impact velocity (m/s)

10 12.5 15 17.5 20 22.5 25 27.5 30

to an impact velocity of 25.0 m/s, the ultimate capacity of the N1 Wall reduces to 17.8 kN, while the corresponding lateral displacement increases to 53.2 mm. This indicates that the deformability of the shear wall increases with the loss of the end stud. In the N2 Wall, the lateral load carrying capacity reduces from 30.7 kN to 24.4 kN when the end

0.2

0 0 2.5 5 7.5



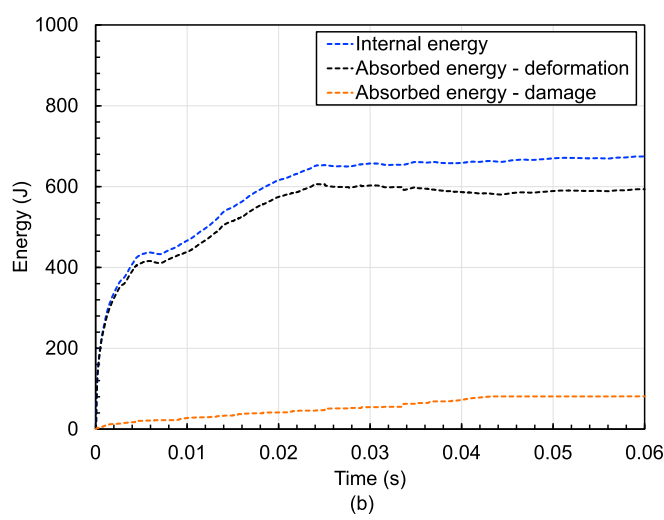


**Fig. 9.** Time history of energy distribution during the simulation of the N1 Wall subjected to debris impact with a velocity of 20.0 m/s.

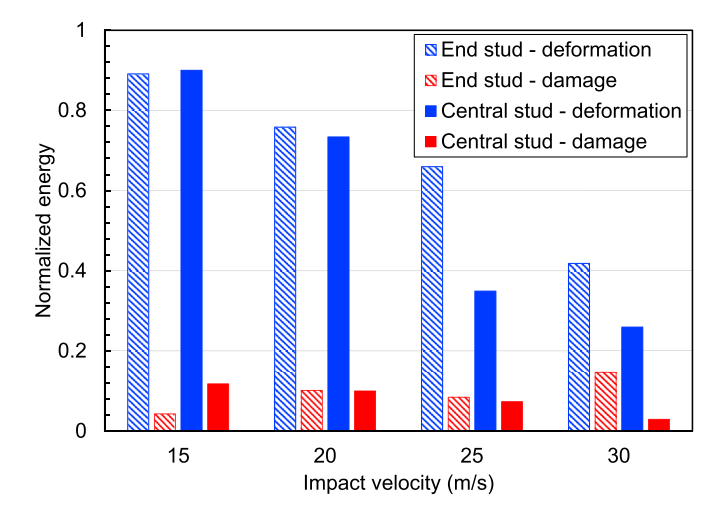


Fig. 10. Effect of impact location on the energy absorption of the N1 Wall.

stud is damaged due to an impact velocity of 25.0 m/s. The displacement corresponding to the ultimate load carrying capacity is also shifted from 50.0 mm to 54.8 mm. For the N3 Wall, the ultimate load carrying capacity reduces from 41.0 kN to 28.6 kN when the end stud is damaged

**Table 3**Effect of angle of attack on the debris penetration depth for impact on the end stud of the three shear walls under an impact velocity of 20.0 m/s.

Debris Penetration Depth (mm)					
Angle of Attack	N1 Wall	N2 Wall	N3 Wall		
90°	146.3	148.2	58.7		
75°	140.7	137.9	56.7		
60°	126.8	123.1	53.7		
45°	105.4	96.5	51.0		

**Table 4**Effect of moisture content on the debris penetration depth for impact on the end stud of the N1 Wall.

Moisture Content	Impact Velocity (m/s)				
	5.0	10.0	15.0	20.0	25.0
5%	25.1	59.1	95.6	Penetration	Penetration
10%	26.1	60.8	95.9	145.9	Penetration
15%	26.5	61.8	96.6	153.9	Penetration
20%	28.3	63.7	96.7	164.5	185.5

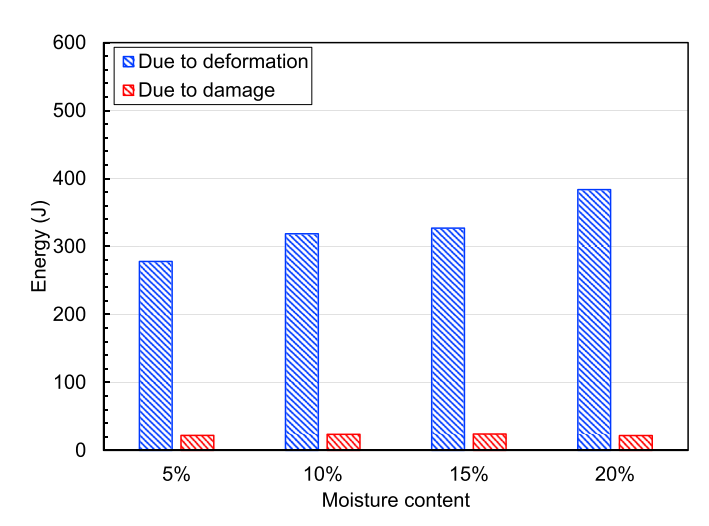


Fig. 11. Effect of moisture content on the energy absorbed by the end stud in the N1 Wall for an impact velocity of 20.0~m/s.

due to an impact velocity of 30.0 m/s. With a trend consistent with the N1 and N2 Walls, the lateral displacement corresponding to the ultimate load carrying capacity of the N3 Wall increases from 47.6 mm to 56.8 mm after experiencing impact-induced damage. The additional displacement required to accommodate the same lateral load highlights how the displacement-sensitive structural and non-structural components of a building can become vulnerable to wind-induced damage.

Considering all the factors that contribute to the assessment of wood frame shear walls located in the regions exposed to severe windstorms, a multi-hazard capacity loss index ( $C_{MH}$ ) is introduced to quantify what percentage of the original capacity is lost due to windborne debris impact:

$$C_{MH} = \left(1 - \frac{P_r}{P_{max}}\right) \tag{4}$$

where  $P_{max}$  and  $P_r$  are the lateral load carrying capacity of the intact and damaged shear wall, respectively. When the shear wall is in the undamaged condition,  $C_{MH}$  is equal 0. This capacity loss index, however, increases when the shear wall sustains debris-induced damage, which adversely affects the in-plane lateral load carrying capacity.

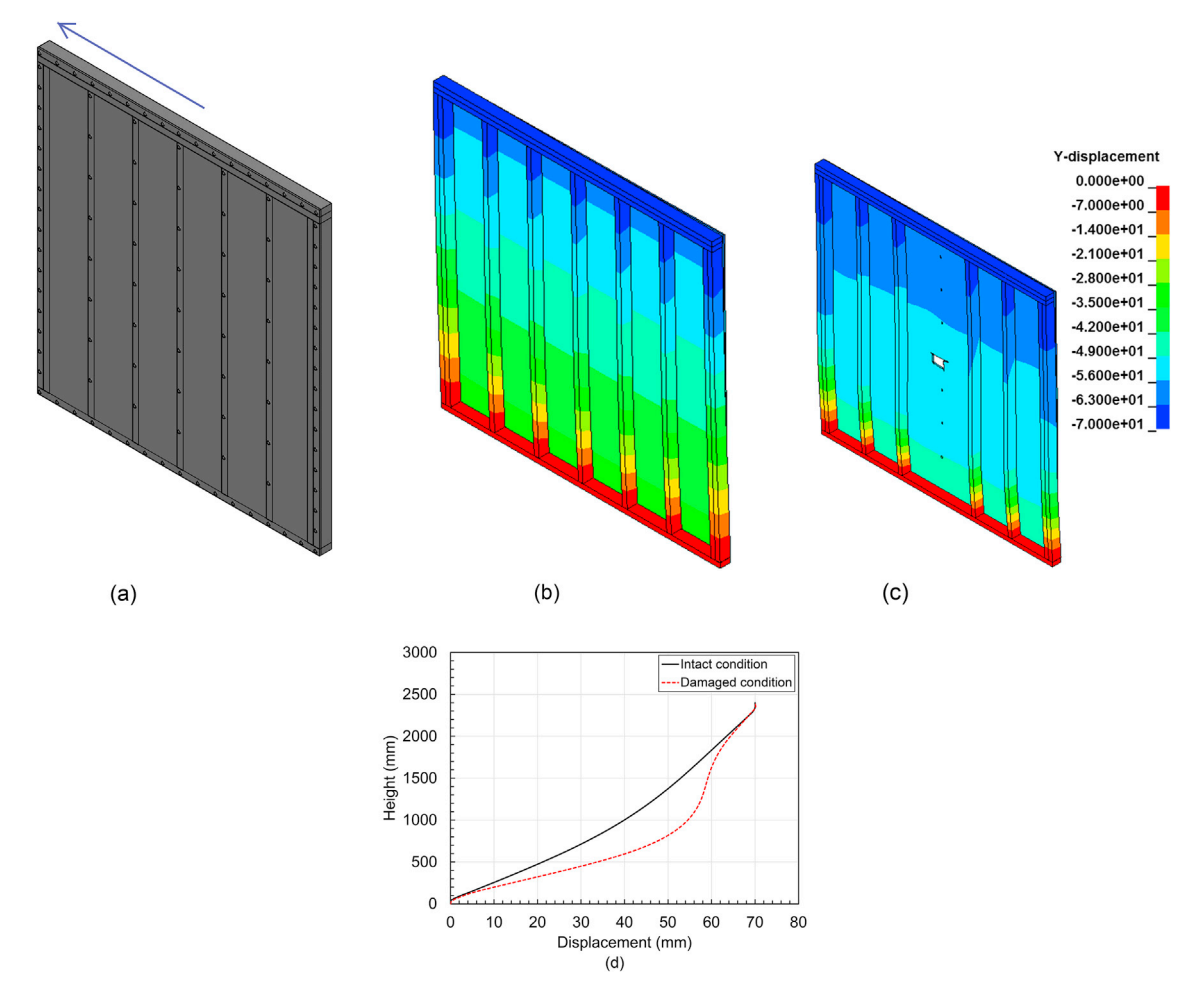


Fig. 12. (a) Schematic illustration of the in-plane lateral load applied to the top of the N1 Wall, (b) and (c) deformed shape of the N1 Wall under a lateral displacement of 70 mm in the intact and damaged condition, respectively, and (d) comparison of the displacement profile along the height of the N1 Wall under the lateral displacement of 70 mm.

Upon extracting the residual capacity of the N1, N2, and N3 Walls from the pushover analyses conducted on the walls damaged with debris impact under velocities ranging from 5.0 m/s to 30.0 m/s (in 5.0 m/s intervals), the introduced multi-hazard capacity loss index is calculated for both central and end studs (Fig. 14). For impact at the end stud, damage is found to increase with increasing the impact velocity from 5.0 m/s to 30.0 m/s. As the end stud is detached from the N1 Wall at the impact velocity of 25.0 m/s (and above), a similar percentage of capacity loss is obtained for both 25.0 m/s and 30.0 m/s impact velocities. As shown in Fig. 14(a), the maximum capacity loss in the N1 Wall is found to be 29.4% when the end stud is fully detached from the shear wall. On the other hand, the maximum capacity loss when the central stud is detached from the same wall is only 4.7%. This difference can be attributed to the difference in the nail spacing at the end and central studs. Fig. 14(b) shows the variation of the percentage of capacity loss as a function of impact velocity for the N2 Wall. For impact at the end stud, the capacity loss increases from 0.2% to 20.0% with increasing the impact velocity from 5.0 m/s to 30.0 m/s. Due to the consistent spacing of nails in all the studs, damage to the N2 Wall is reduced when the end stud is detached. Fig. 14(c) reports the percentage of capacity loss for the N3 Wall. Due to the dense spacing of the nails at the end studs, the residual lateral load carrying capacity is mainly governed by damage to the end studs. The recorded loss is found to increase from 0.5% to 31.0% with increasing the impact velocity from 5.0 m/s to 30.0 m/s at the end studs. For the range of impact velocities between 5.0 m/s and 20.0 m/s, the damage is not significant. This confirms the importance of nail spacing in improving the resistance of shear walls to impact loads. When the end stud is completely detached, a capacity loss of 31% is observed in the N3 Wall, as compared to 29% and 20% for the N1 and N2 Walls, respectively. This highlights the fact that the loss of lateral load carrying capacity is directly proportional to the failure of sheathing to frame connections.

# 6. Conclusions

This study investigated the structural response of wood frame shear walls subjected to windborne debris impact and lateral wind loads. While the studies available in the literature were primarily focused on the assessment of wood frame shear walls under only one of these two extreme events, there was a research gap regarding the performance of this important category of structural systems under wind and windborne debris impact, which often occur together during severe windstorms. Noting that the damage caused by windborne debris impact can significantly reduce the capacity of shear walls subjected to in-plane lateral loads, a multi-hazard computational framework was developed in the current study. Through this framework, the vulnerability of a set of representative wood frame shear walls was studied by simulating the windborne debris impact and then capturing how the impact-induced damage influences the capacity of wood frame shear walls to resist lateral wind loads. After validating the numerical models, the performance of shear walls was examined using various performance measures, such as penetration depth, absorbed energy, and deformed shape. The simulations also unveiled the effect of various contributing factors, such

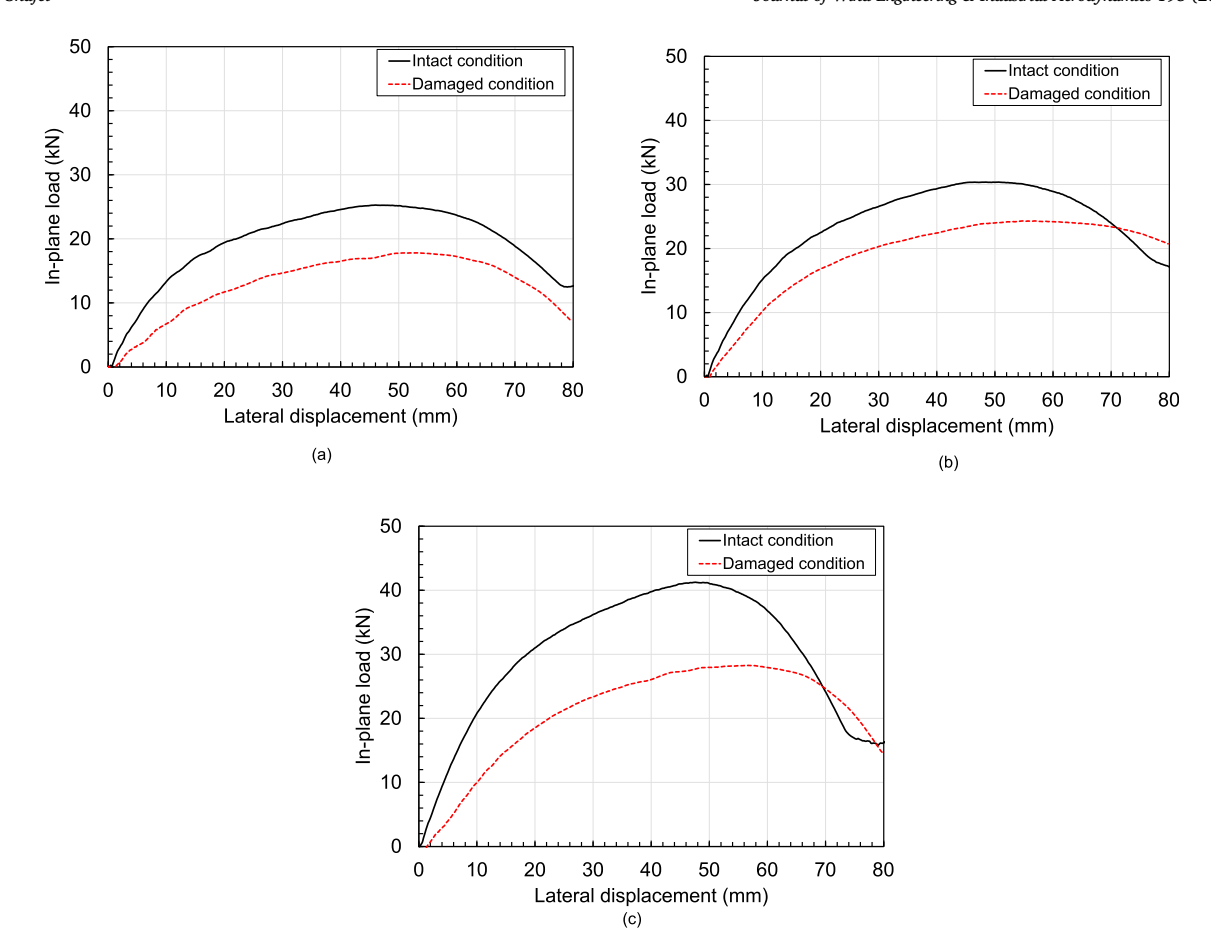


Fig. 13. Comparison of the pushover curves obtained for the wood frame shear walls with and without impact-induced damage at the end stud: (a) N1, (b) N2, and (c) N3 Wall.

as impact location, angle of attack, nail spacing, and moisture content. The simulations were further extended to quantify the extent of damage by evaluating the residual pushover capacity of the shear walls under consideration, leading to introducing a multi-hazard capacity loss index. Based on the simulation results, the loss of lateral load carrying capacity was primarily due to damage to the studs. This was the main reason that the impact on the shear walls was assumed aligned with a stud, as such an assumption leads to the most extreme scenarios. The main findings and conclusions of the current study are as follows:

- The damage accumulated in the wood frame shear walls due to debris impact was found to greatly depend on the structural details of the studs and the sheathing panel. Upon a direct debris impact to the sheathing panel, a punching shear failure was observed under the impact velocities as low as 10.0 m/s. For impact to the studs, however, impact velocities below 25.0 m/s were tolerated, owing to the deformation of the studs. Ultimately, the impacted studs were detached from the rest of the wall, leading to a failure of the stud to sheathing panel connections.
- The energy absorption characteristics were reported as a measure of how the penetration resistance of the wood frame shear walls is governed by deformation and structural damage. Under low impact velocities in the range of 5.0 m/s to 15.0 m/s, the energy absorbed due to deformation dominated. As the impact velocities exceeded 15.0 m/s, however, the energy absorbed due to structural damage to the studs significantly increased. Comparing to the end studs, the central studs were found to experience failure at lower impact velocities, mainly because of their lower energy absorption capacity.

- The frame to sheathing panel connections significantly affected the impact resistance and lateral load carrying capacity of the wood frame shear walls. For impact to the end studs, the penetration depth was found to reduce by at least 60% with changing the nail spacing from 150 mm to 75 mm. A similar improvement was observed in the lateral load carrying capacity of the shear walls under consideration.
- The simulations performed with four moisture contents, ranging from 5% to 20%, showed the importance of this factor when predicting the penetration resistance of wood frame shear walls. The nature of the structural response of the wood frame shear walls was observed to change as the moisture content increased to above 10%. In particular, higher moisture contents resulted in more deformations in the studs (prior to failure). This was confirmed through monitoring the absorbed energy, which was consistently increased by up to 38% with increasing the moisture content from 5% to 20%.
- The effect of windborne debris impact on the performance of shear walls subjected to in-plane lateral loads was quantified by calculating their residual load carrying capacity. Based on the pushover analyses conducted on the intact and damaged shear walls, it was found that the lateral load carrying capacity decreases up to 31% in the shear walls that were damaged with debris impact velocities greater than 15.0 m/s.
- With taking into consideration the effects of two extreme events, a realistic prediction of the percentage of capacity loss due to windborne debris impact is deemed a critical input for the multi-hazard design and assessment of wood frame shear walls in the regions that often experience hurricanes and tornados. The outcome of this effort can be further employed to inform the allocation of resources

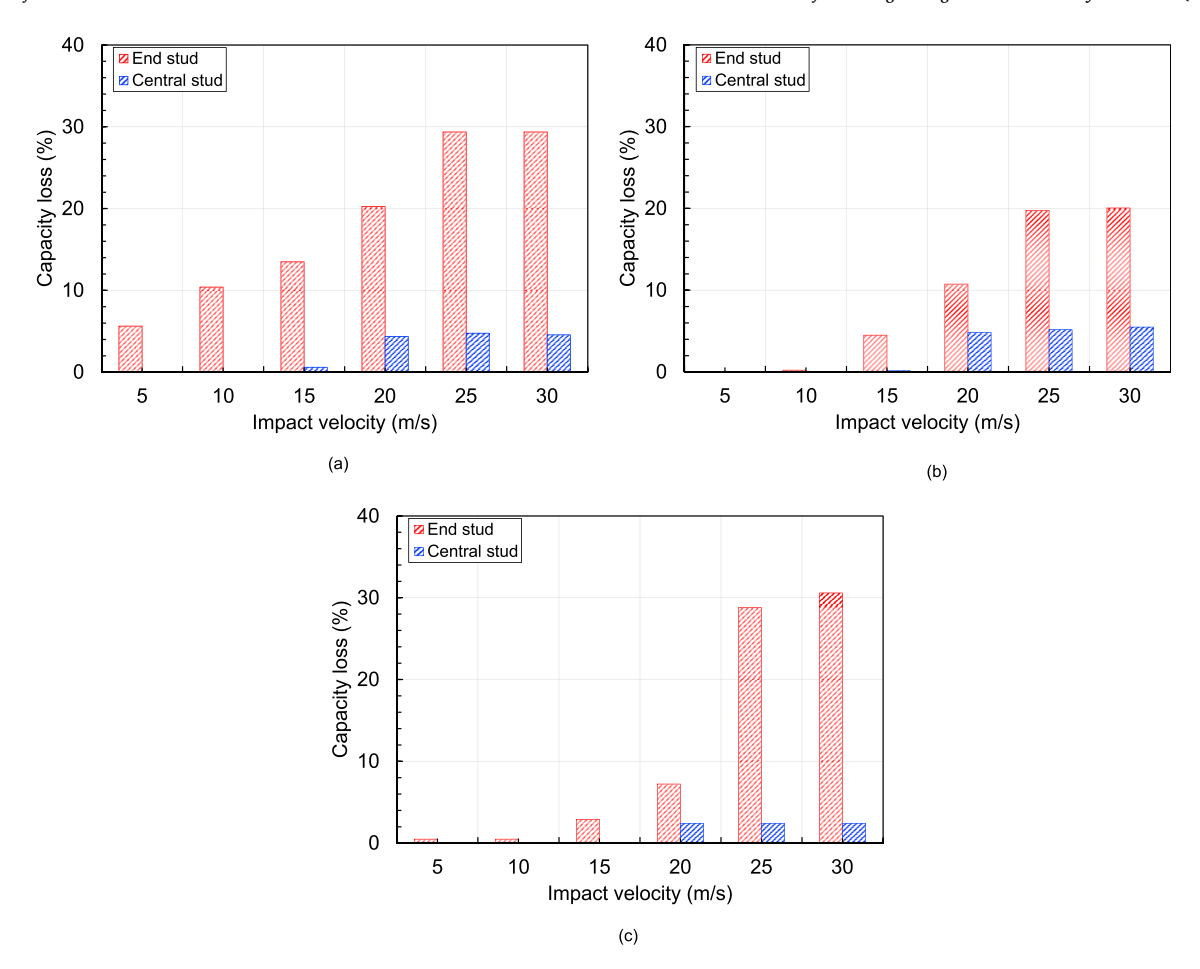


Fig. 14. Loss of the original capacity as a function of impact velocity for (a) N1, (b) N2, and (c) N3 Wall.

and prioritization of activities essential to mitigate the consequences of severe windstorms.

## **Declaration of Competing interest**

The authors have no conflict of interest to report.

# CRediT authorship contribution statement

**Dikshant Saini:** Methodology, Software, Validation, Investigation, Writing - original draft. **Behrouz Shafei:** Conceptualization, Methodology, Investigation, Writing - review & editing, Funding acquisition, Supervision.

# Acknowledgement

The research study, results of which reported in this manuscript, was partially sponsored by the U.S. National Science Foundation under Awards No. 1826356 and 1827774. The authors would like to acknowledge and thank the sponsor for this support. Opinions, findings, and conclusions expressed in this manuscript are of the authors and do not necessarily reflect those of the U.S. National Science Foundation.

# References

Alphonso, T.C., Barbato, M., 2014. Experimental fragility curves for aluminum storm panels subject to windborne debris impact. J. Wind Eng. Ind. Aerodyn. 134, 44–55.
 Andersen, A., Pesavento, U., Wang, Z.J., 2005. Unsteady aerodynamics of fluttering and tumbling plates. J. Fluid Mech. 541, 65–90.

ASTM, 2013. Standard Test Method for Performance of Exterior Windows, Curtain Walls, Doors, and Impact Protective Systems Impacted by Missile(s) and Exposed to Cyclic Pressure Differentials (West Conshohocken, PA).

Baker, C.J., 2007. The debris flight equations. J. Wind Eng. Ind. Aerodyn. 95, 329–353.
 Baker, C.J., Sterling, M., 2017. Modelling wind fields and debris flight in tornadoes.
 J. Wind Eng. Ind. Aerodyn. 168, 312–321.

Blasetti, A.S., Hoffman, R.M., Dinehart, D.W., 2008. Simplified hysteretic finite-element model for wood and viscoelastic polymer connections for the dynamic analysis of shear walls. J. Struct. Eng. 134, 77–86.

Chen, W., Hao, H., 2015. Performance of structural insulated panels with rigid skins subjected to windborne debris impacts–Experimental investigations. Constr. Build. Mater. 77, 241–252.

Chen, W., Hao, H., 2014. Experimental and numerical study of composite lightweight structural insulated panel with expanded polystyrene core against windborne debris impacts. Mater. Des. 60, 409–423.

Durham, J.P., 1998. Seismic Response of Wood Shear Walls with Oversized Oriented Strand Board Panels. MASc thesis. Univ. of British Columbia, Vancouver B.C., Canada.

Durham, J., Lam, F., Prion, H.G.L., 2001. Seismic resistance of wood shear walls with large OSB panels. J. Struct. Eng. 127, 1460–1466.

FBC, 2017. Florida Building Code 2017, Building. International Code Council, Inc, USA. FEMA, 2015. Safe Rooms for Tornadoes and Hurricanes: Guidance for Community and Residential Safe Rooms. FEMA P-361, Washington, DC.

FEMA, 2019. Hurricane Harvey in Texas: Building Performance Observations, Recommendations, and Technical Guidance. FEMA P-2022, Washington, DC. Folz, B., Filiatrault, A., 2001. Cyclic analysis of wood shear walls. J. Struct. Eng. 127, 433-441.

Gatto, K., Uang, C.-M., 2003. Effects of loading protocol on the cyclic response of woodframe shearwalls. J. Struct. Eng. 129, 1384–1393.

Glass, S.V., TenWolde, A., 2007. Review of In-Service Moisture and Temperature Conditions in Wood-Frame Buildings. U.S. Department of Agriculture, Forest Service, Forest Products Laboratory, Madison, WI. General Technical Report FPL-GTR-174.
Gupta, A.K., Kuo, G.P., 1985. Behavior of wood-framed shear walls. J. Struct. Eng. 111, 1722–1733.

Hao, H., Chen, W., Chen, S., Meng, Q., 2015. Finite element analysis of structural insulated panel with OSB skins against windborne debris impacts. In: 1st Pan-American Congress on Computational Mechanics (PANACM).

Herbin, A.H., Barbato, M., 2012. Fragility curves for building envelope components subject to windborne debris impact. J. Wind Eng. Ind. Aerodyn. 107, 285–298. Holmes, J.D., 2004. Trajectories of spheres in strong winds with application to windborne debris. J. Wind Eng. Ind. Aerodyn. 92, 9–22.

- Holmes, J.D., Letchford, C.W., Lin, N., 2006. Investigations of plate-type windborne debris—Part II: computed trajectories. J. Wind Eng. Ind. Aerodyn. 94, 21–39.
- ICC, 2014. In: Standard for Residential Construction in High-Wind Regions, ICC 600-20 (Washington, D.C).
- Jin, C., Xu, K., 2008. Numerical study of the unsteady aerodynamics of freely falling plates. Commun. Comput. Phys. 3, 834–851.
- Kakimpa, B., Hargreaves, D.M., Owen, J.S., 2012a. An investigation of plate-type windborne debris flight using coupled CFD-RBD models. Part I: model development and validation. J. Wind Eng. Ind. Aerodyn. 111, 95–103.
- Kakimpa, B., Hargreaves, D.M., Owen, J.S., 2012b. An investigation of plate-type windborne debris flight using coupled CFD–RBD models. Part II: free and constrained flight. J. Wind Eng. Ind. Aerodyn. 111, 104–116.
- Kordi, B., Kopp, G.A., 2011. Effects of initial conditions on the flight of windborne plate debris. J. Wind Eng. Ind. Aerodyn. 99, 601–614.
- Kordi, B., Traczuk, G., Kopp, G.A., 2010. Effects of wind direction on the flight trajectories of roof sheathing panels under high winds. Wind Struct. 13, 145–167.
- Lafontaine, A., Chen, Z., Doudak, G., Chui, Y.H., 2017. Lateral behavior of light wood-frame shear walls with gypsum wall board. J. Struct. Eng. 143, 4017069.
- Lam, F., Prion, H.G.L., He, M., 1997. Lateral resistance of wood shear walls with large sheathing panels. J. Struct. Eng. 123, 1666–1673.
- Lin, N., Holmes, J.D., Letchford, C.W., 2007. Trajectories of wind-borne debris in horizontal winds and applications to impact testing. J. Struct. Eng. 133, 274–282.
- Lin, N., Letchford, C., Holmes, J., 2006. Investigation of plate-type windborne debris. Part

  I. Experiments in wind tunnel and full scale. J. Wind Eng. Ind. Aerodyn. 94, 51–76.
- I. Experiments in wind tunnel and full scale. J. Wind Eng. Ind. Aerodyn. 94, 51–76 LSTC, 2016. LS-DYNA Theory Manual. Livermore Software Technology Corporation, Livermore, CA.
- Marshall, T.P., 2002. Tornado damage survey at Moore, Oklahoma. Weather Forecast. 17, 582–598.
- Meng, Q., Hao, H., Chen, W., 2016a. Laboratory test and numerical study of structural insulated panel strengthened with glass fibre laminate against windborne debris impact. Constr. Build. Mater. 114, 434–446.
- Meng, Q., Hao, H., Chen, W., 2016b. Experimental and numerical study of basalt fibre cloth strengthened structural insulated panel under windborne debris impact. J. Reinf. Plast. Compos. 35, 1302–1317.
- Murray, Y.D., 2007. Manual for LS-DYNA Wood Material Model 143. Report FHWA-HRT-04-097. Federal Highway Administration. Washington, DC.
- Noda, M., Nagao, F., 2010. Simulation of 6DOF motion of 3D flying debris. In:

  Proceedings of 5th International Symposium on Computational Wind Engineering.

- Oliver, C., Hanson, C., 1992. Failure of residential building envelopes as a result of hurricane Andrew in dade county, Florida. In: Hurricanes of 1992: Lessons Learned and Implications for the Future, pp. 396–508.
- Otkur, M., 2010. Impact Modeling and Failure Modes of Composite Plywood.
- Pathirana, M., Lam, N., Perera, S., Zhang, L., Ruan, D., Gad, E., 2017. Damage modelling of aluminium panels impacted by windborne debris. J. Wind Eng. Ind. Aerodyn. 165, 1–12
- Pei, S., van de Lindt, J.W., Wehbe, N., Liu, H., 2012. Experimental study of collapse limits for wood frame shear walls. J. Struct. Eng. 139, 1489–1497.
- Reddy, T.Y., Wen, H.M., Reid, S.R., Soden, P.D., 1998. Penetration and perforation of composite sandwich panels by hemispherical and conical projectiles. J. Press. Vessel Technol. 120, 186–194.
- Richards, P.J., Williams, N., Laing, B., McCarty, M., Pond, M., 2008. Numerical calculation of the three-dimensional motion of wind-borne debris. J. Wind Eng. Ind. Aerodyn. 96, 2188–2202.
- Saini, D., Shafei, B., 2018. Vulnerability of metal roof decking systems subjected to windborne debris impact. In: 5th American Association for Wind Engineering Workshop, Miami, FL.
- Saini, D., Shafei, B., 2019a. Performance of concrete-filled steel tube bridge columns subjected to vehicle collision. J. Bridge Eng. 24 (8), 1–13.
- Saini, D., Shafei, B., 2019b. Investigation of concrete-filled steel tubes strengthened with CFRP against impact loads. J. Compos. Struct. 208, 744–757.
- Saini, D., Shafei, B., 2019c. Concrete constitutive models for low velocity impact simulations. Int. J. Impact Eng. 132, 103329, 1-13.
- Sherwood, G.E., 1985. Condensation Potential in High Thermal Performance Walls. Forest Products Laboratory, Madison WI. Report No. FPL-455.
- Tachikawa, M., 1988. A method for estimating the distribution range of trajectories of wind-borne missiles. J. Wind Eng. Ind. Aerodyn. 29, 175–184.
- Tachikawa, M., 1983. Trajectories of flat plates in uniform flow with application to windgenerated missiles. J. Wind Eng. Ind. Aerodyn. 14, 443–453.
- Tissell, J.R., 1993. Wood Structural Panel Shear Walls. American Plywood Association (APA) –The Engineered Wood Association, Tacoma, WA. Report 154.
- Van De Lindt, J.W., 2004. Evolution of wood shear wall testing, modeling, and reliability analysis: Bibliography. Pract. Period. Struct. Des. Constr. 9, 44–53.
- Visscher, B.T., Kopp, G.A., 2007. Trajectories of roof sheathing panels under high winds. J. Wind Eng. Ind. Aerodyn. 95, 697–713.
- Wang, R., Xiao, Y., Li, Z., 2017. Lateral loading performance of lightweight glubam shear walls. J. Struct. Eng. 143, 4017020.
- Wills, J.A.B., Lee, B.E., Wyatt, T.A., 2002. A model of wind-borne debris damage. J. Wind Eng. Ind. Aerodyn. 90, 555–565.